Journal of Alloys and Compounds 504S (2010) S487–S490

Contents lists available at ScienceDirect

Journal of Alloys and Compounds

journal homepage: www.elsevier.com/locate/jallcom

Effect of Nb on microstructure and mechanical properties of ultrafine eutectic Fe–Ni–B–Si composites

D.H. Pi[a], G.A. Song[a], J.H. Han[a], J.M. Park[b], G.R. Lim[c], D.H. Kim[c], S. Yi[d], S.H. Yi[e], N.S. Lee[a], Y. Seo[a], K.B. Kim[a,*]

[a] Faculty of Nanotechnology and Advanced Materials Engineering, Sejong University, 98 Gunja-dong, Gwangjin-gu, Seoul 143-747, Republic of Korea
[b] IFW Dresden, Institute for Complex Materials, D-01171 Dresden, Germany
[c] Center for Non-crystalline Materials, Department of Metallurgical Engineering, Yonsei University, Republic of Korea
[d] Department of Materials Science and Metallurgy, Kyungpook National University, 1370 Sankyuk-dong, Buk-gu, Daegu 702-701, Republic of Korea
[e] Technical Research Laboratories, POSCO, 1, Goedong-dong, Nam-Gu, Pohang, Gyeongbuk 790-785, Republic of Korea

ARTICLE INFO

Article history:
Received 22 July 2009
Received in revised form
30 December 2009
Accepted 10 February 2010
Available online 18 February 2010

Keywords:
Composite materials
Mechanical properties
Microstructure

ABSTRACT

Microstructural investigation on a series of $(Fe_{65.8}Ni_{14.1}B_{14.1}Si_6)_{100-x}Nb_x$ alloys with $x = 0$, 2, 4, 6 and 8 reveals that Nb addition leads to modify the constitutive phase and morphology of ultrafine eutectic structure. The microstructural change from bimodal to irregular eutectic structures by addition of Nb has a strong influence to deteriorate the macroscopic plasticity. The bimodal structure and eutectic colony morphology is considered to be an important factor for enhancing both strength and plasticity.

1. Introduction

Bulk metallic glasses (BMGs) have been highlighted due to unique physical, chemical and mechanical properties [1–4]. However, such high strength BMGs often exhibit a catastrophic failure without macroscopic plastic strain due to an occurrence of shear localization upon deformation [5,6]. In order to enhance the room temperature plasticity of the BMGs, so far several investigations have been performed by introducing micron-scale primary dendrite and nano-scale precipitate [7–9]. Nb-reinforced Mg-based BMGs, for example, exhibit a great combination of high strength of ~900 MPa, and an enhanced plasticity of ~12% [10].

Similarly, dendrite–eutectic composites consisting of micron-scale dendrite embedded by ultrafine eutectic matrix have been recently developed in Ti- [11,12], Zr- [13], Mg- [14,15] and Fe- [16,17] based alloys. For example, the Fe-based dendrite–eutectic composites with micron-scale dendrite exhibit high yield strength of 1.5–1.9 GPa combined with improved plasticity of 7–12% [17]. Systematic investigations on deformation behavior of the Fe–Zr dendrite–eutectic composites reveal that the mechanical properties are governed by the volume fraction of the micron-scale dendrites and ultrafine eutectic matrix, implying inevitable sacrifice of either strength or plasticity in the dendrite–eutectic composites [17].

Recently, there is an interesting finding that bimodal eutectic composites in Ti- [18,19], Mg- [20] based alloys comprising micron-scale dendrite homogeneously embedded by bimodal eutectic structure with spatial, i.e. length scale and morphology, and structural heterogeneity, i.e. constitutive phases, possess a great combination of the strength and plasticity. Detailed investigations on the deformation behavior of the Ti–Fe–Sn bimodal eutectic composite reveal that the interface between eutectic structures acts as a nucleation site for shear bands and different eutectic structures effectively inhibit the propagation of shear bands [19]. This scenario suggests that the bimodal eutectic structure can be considered as a promising concept to enhance the mechanical properties of the eutectic composite. However, only a few reports on the formation and the modulation of bimodal eutectic structure in Fe-based alloys are available so far.

In the present paper, we systematically investigate microstructural evolution as adding Nb content into Fe–Ni–B–Si bimodal ultrafine eutectic composite composed of fully eutectic structure without micro-scale dendrite. Since Nb is considered as γ-Fe, Nb is selected as an additional element. Also, we focus on effect of the microstructural change on the mechanical properties of the present alloys.

* Corresponding author. Tel.: +82 2 3408 3690; fax: +82 2 3408 3664.
E-mail addresses: kbkim@sejong.ac.kr, kibuem@googlemail.com (K.B. Kim).

0925-8388/$ – see front matter © 2010 Elsevier B.V. All rights reserved.
doi:10.1016/j.jallcom.2010.02.066

2. Experimental procedure

The Fe–Ni–B–Si–Nb alloys were prepared by arc melting with a mixture of high purity elements (purity > 99.8 wt%) under Ti-gettered argon atmosphere and each alloy re-melted at least three times to ensure homogeneity. Rods specimen with 2 mm diameter and 50 mm length were casted into cylindrical copper mold. The microstructure of the samples was analyzed using scanning electron microscopy (SEM, JEOL, JSM-6390). X-ray diffraction with monochromatic Cu Ka radiation (XRD, Rigaku RINT2000) and transmission electron microscopy (TEM, JEM2010) experiments were used for the structural characterization. Thin foils for TEM were prepared by ion milling (Gatan, model 600). In order to estimate the mechanical properties, cylindrical specimens with 2 mm diameter and 4 mm length were prepared and tested under room temperature compression at an initial strain rate of $1 \times 10^{-3}\ s^{-1}$.

3. Results and discussion

Fig. 1 shows that X-ray diffraction (XRD) patterns of as-cast $(Fe_{65.8}Ni_{14.1}B_{14.1}Si_6)_{100-x}Nb_x$ alloys with $x = 0$, 2, 4, 6 and 8. The main sharp diffraction peaks of the $Fe_{65.8}Ni_{14.1}B_{14.1}Si_6$ alloy in Fig. 1(a) can be identified as a mixture of a bcc α-Fe ($Im\bar{3}m$), bct $(Fe,Ni)_2B$ ($I4/mcm$) and fcc $(Fe,Ni)_{23}B_6$ ($Fm3m$) phases. However, as the amount of additional Nb content increases the main diffraction patterns of the $(Fe_{65.8}Ni_{14.1}B_{14.1}Si_6)_{100-x}Nb_x$ alloys with $x = 2$, 4, 6 and 8 in Fig. 1(b)–(e) gradually vary, implying that the addition of Nb content induces significant phase change. Fig. 1(b) reveals that the relative intensity of α-Fe phase considerably increases, whereas that of both $(Fe,Ni)_2B$ and $(Fe,Ni)_{23}B_6$ phases decrease with increasing Nb content. Moreover, diffraction traces of fcc γ-Fe ($Fm\bar{3}m$) phase appear. Therefore, it is believed that small amount of Nb addition facilitates formation of γ-Fe. With further increasing Nb content up to 8 at.%, the diffraction intensity of α-Fe and γ-Fe gradually rises whereas that of $(Fe,Ni)_{23}B_6$ phase decreases as shown in Fig. 1(c)–(e). No visible trances of the $(Fe,Ni)_2B$ phase can be observable in Fig. 1(c)–(e). Hence, these result strongly support that additional Nb not only suppresses the formation of both $(Fe,Ni)_2B$ and $(Fe,Ni)_{23}B_6$ phases but also stimulates α-Fe and γ-Fe phases.

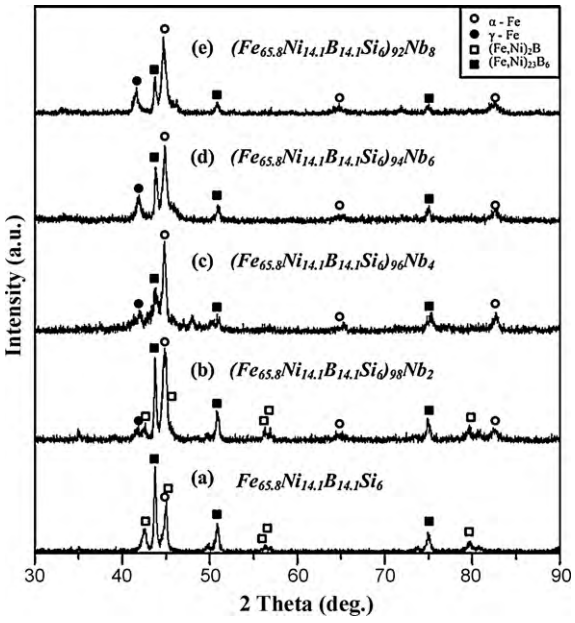

Fig. 1. XRD patterns of the $(Fe_{65.8}Ni_{14.1}B_{14.1})_{100-x}Nb_x$ ultrafine eutectic composites with $x = 0$, 2, 4, 6 and 8.

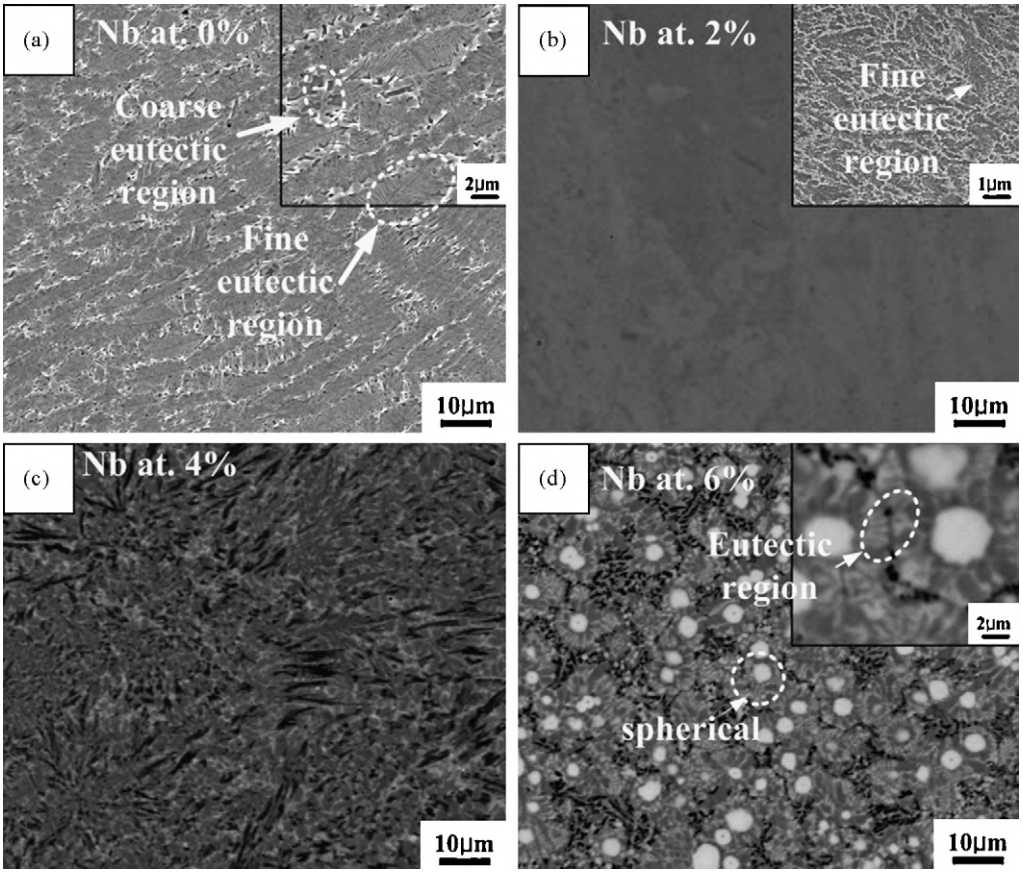

Fig. 2. SEM secondary electron (a) and (b) and back scattering images (c) and (d) obtained from the $(Fe_{65.8}Ni_{14.1}B_{14.1})_{100-x}Nb_x$ ultrafine eutectic composites with $x = 0$, 2, 4, 6 and 8.

Fig. 2(a) and (b) shows SEM secondary electron images and back scattering images (Fig. 2(c) and (d)) obtained from as-cast $(Fe_{65.8}Ni_{14.1}B_{14.1}Si_6)_{100-x}Nb_x$ (x = 0, 2, 4 and 6) alloys. The SEM image of the $Fe_{65.8}Ni_{14.1}B_{14.1}Si_6$ alloy in Fig. 2(a) displays fully eutectic structure without micron-scale dendrite. The inset SEM image at higher magnification in Fig. 2(a) clearly reveals bimodal eutectic structure consisting of fine lamellar region with lamellar spacing of 300–400 nm and coarse irregular region. Furthermore, fine lamellar region with spherical morphology is surrounded by coarse irregular region. The spherical colony size is measured to be 20–30 μm. The SEM image of $(Fe_{65.8}Ni_{14.1}B_{14.1}Si_6)_{98}Nb_2$ alloy in Fig. 2(b) shows the colony size significantly decreases down to 1–5 μm whereas there is no clear change on the lamellar spacing of both fine and coarse eutectic structures in the alloy. BSE image in Fig. 2(c) obtained from as-cast $(Fe_{65.8}Ni_{14.1}B_{14.1}Si_6)_{96}Nb_4$ alloy displays that microstructure is quite different to that of the $(Fe_{65.8}Ni_{14.1}B_{14.1}Si_6)_{100-x}Nb_x$ (x = 0 and 2) in Fig. 2(a) and (b). By combining results from SEM and XRD γ-Fe, α-Fe and $(Fe,Ni)_{23}B_6$ phases is considered to display white, gray black contrast in BSE mode, respectively. The BSE image of as-cast $(Fe_{65.8}Ni_{14.1}B_{14.1}Si_6)_{94}Nb_6$ alloy in Fig. 2(d) exhibits coarse irregular eutectic region and lamellar eutectic region embedding micron primary dendrite with bright contrast. The size of primary dendrite and lamellar spacing of the lamellar eutectic region in Fig. 2(d) is measured to ~2 μm and is ~1 μm, respectively. It is clear that the volume faction of the γ-Fe phase with bright contrast in Fig. 2(c) and (d) significantly increases, which is in good agreement with the result from XRD in Fig. 1.

Fig. 3(a) shows a SEM back scattering image, TEM bright-field image Fig. 3(b), and selected area diffraction patterns (SADPs) Fig. 3(c)–(e) of as-cast $(Fe_{65.8}Ni_{14.1}B_{14.1}Si_6)_{96}Nb_4$ alloy. The TEM bright-field image in Fig. 3(b) obtained from the region denoted by white circle in Fig. 3(a) reveals that the $(Fe_{65.8}Ni_{14.1}B_{14.1}Si_6)_{94}Nb_6$ alloy consists of three different regions which are recognized from contrast difference (bright, gray and dark). The SADPs in Fig. 3(c) obtained from the bright area in Fig. 3(b) corresponds to the [1 1 1] zone axis of the α-Fe phase. The SADPs in Fig. 3(d) and (e) obtained from the gray and dark area in Fig. 3(b) correspond to [1 1 0] and [0 0 1] zone axes of $(Fe,Ni)_{23}B_6$ and γ-Fe phases, respectively. Therefore, it is clear that the $(Fe_{65.8}Ni_{14.1}B_{14.1}Si_6)_{96}Nb_4$ alloy consists of the α-Fe, $(Fe,Ni)_{23}B_6$ and γ-Fe phases.

Fig. 4 shows compressive engineering strain–stress curves of $(Fe_{65.8}Ni_{14.1}B_{14.1}Si_6)_{100-x}Nb_x$ (x = 0, 2, 4, 6 and 8) alloys. $Fe_{65.8}Ni_{14.1}B_{14.1}Si_6$ alloy, which is composed of fully bimodal eutectic structure without micron-scale primary dendrite, exhibits the large plasticity ε_p of ~11.5% with yield strength σ_y of 1.2 GPa, respectively. $(Fe_{65.8}Ni_{14.1}B_{14.1}Si_6)_{98}Nb_2$ alloy in Fig. 4(b) shows slightly improved yield strength σ_y of 1.6 GPa, and slightly decreased plasticity of ε_p of 5.4%, indicating that mechanical properties of the bimodal eutectic composites can be controlled by size of the eutectic colony. However, the $(Fe_{65.8}Ni_{14.1}B_{14.1}Si_6)_{100-x}Nb_x$ alloys with x = 4, 6 and 8 exhibit the higher yield strength σ_y of 2–2.3 GPa with limited plasticity. Table 1 shows the value of the values of the yield strength σ_y, ultimate compressive strength σ_{max} and compressive plastic strain ε_p for a series of $(Fe_{65.8}Ni_{14.1}B_{14.1})_{100-x}Nb_x$ bimodal ultrafine eutectic alloys with x = 0, 2, 4, 6 and 8.

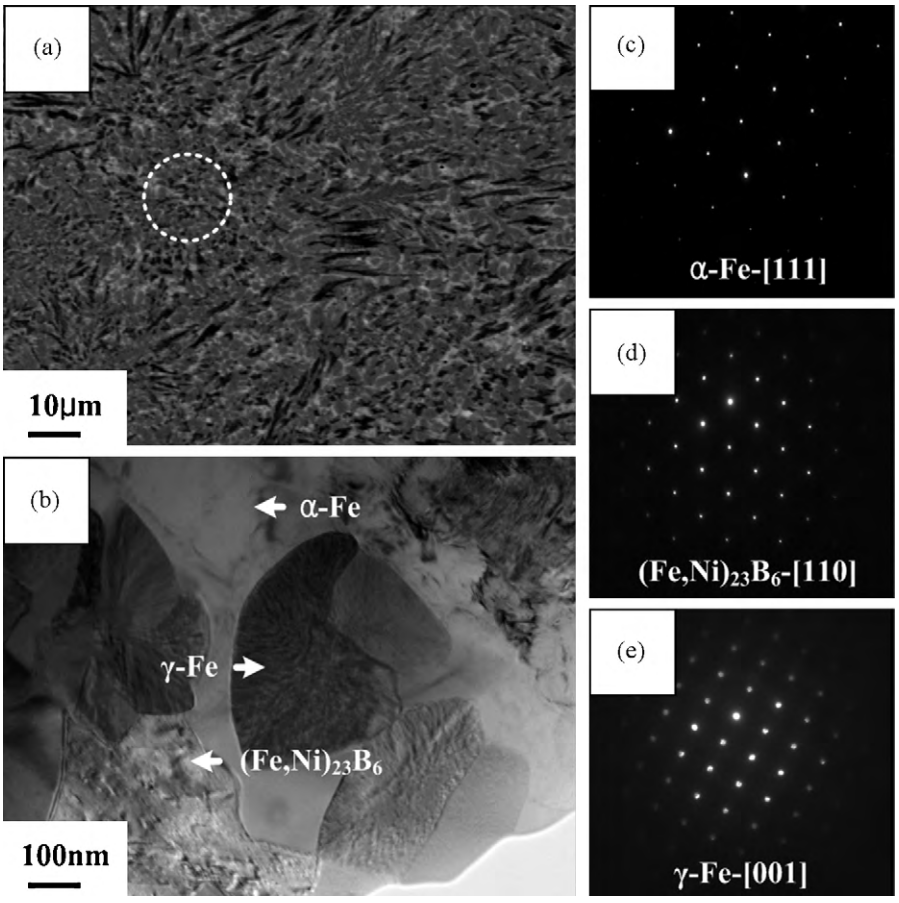

Fig. 3. SEM back scattering electron image (a), TEM bright-field image (b) and selected area diffraction patterns (c)–(e) obtained from the $(Fe_{65.8}Ni_{14.1}B_{14.1}Si_6)_{96}Nb_4$ ultrafine eutectic composite.

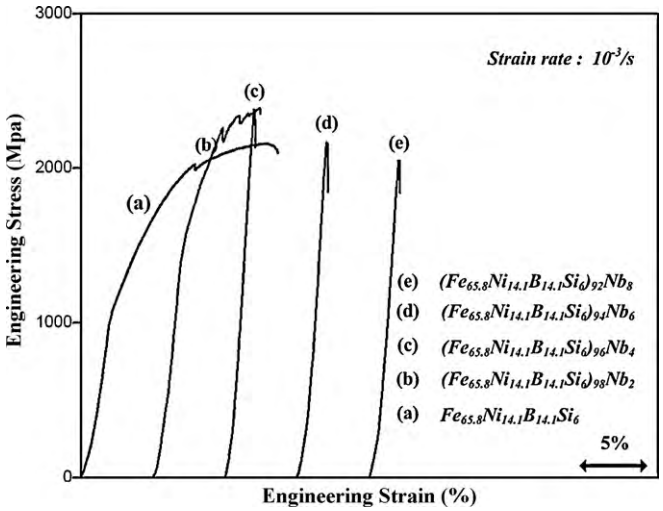

Fig. 4. Stress–strain curves of the $(Fe_{65.8}Ni_{14.1}B_{14.1})_{100-x}Nb_x$ ultrafine eutectic composites with $x = 0$, 2, 4, 6 and 8 under room temperature compression.

Table 1
Mechanical properties (yield stress σ_y, ultimate stress σ_{max} and plastic strain ε_p) of a series of $(Fe_{65.8}Ni_{14.1}B_{14.1})_{100-x}Nb_x$ ultrafine eutectic composites with $x = 0$, 2, 4, 6 and 8 under room temperature compression.

Composition (at.%)	O_y (MPa)	CW (MPa)	Sp (%)
(a) $Fe_{65.8}Ni_{14.1}B_{14.1}Si_6$	1199	2158	11.5
(b) $(Fe_{65.8}Ni_{14.1}Si_6)_{98}Nb_2$	1605	2387	5.4
(c) $(Fe_{65.8}Ni_{14.1}Si_6)_{96}Nb_4$	2379	2380	0.5
(d) $(Fe_{65.8}Ni_{14.1}Si_6)9_4Nb_6$	2164	2164	0.1
(e) $(Fe_{65.8}Ni_{14.1}Si_6)_{92}Nb_8$	2048	2048	0.09

In general, it is well known that mechanical properties of the ultrafine eutectic composite are strongly related to their microstructure, such as length scale, constitutive phase and morphology. For example, it was reported that the plasticity is significantly improved with by modulation of microstructural morphology in Fe- and Ti-based alloys [21,22]. Similarly, the $(Fe_{65.8}Ni_{14.1}B_{14.1})_{100-x}Nb_x$ alloy with $x = 0$ and 2 comprising bimodal eutectic structure with spherical eutectic colony reveal the high strength of 1.1–1.6 GPa combined with improved plasticity of 5–11%. However, further additional Nb leads to microstrctural change including constitutive phase and morphology, resulting in limited plasticity even though $(Fe_{65.8}Ni_{14.1}B_{14.1})_{100-x}Nb_x$ alloys with $x = 4$, 6 and 8 contain large amount of solid solution α-Fe and γ-Fe phases. Therefore, it is believed that the bimodal eutectic structure with spherical morphology is considered as a key factor to improve the both strength and plasticity.

4. Summary

We have systematically investigated microstructural evolution and change of mechanical properties as adding Nb content into $Fe_{65.8}Ni_{14.1}B_{14.1}Si_6$ bimodal eutectic composite. With increasing Nb content, the volume fraction of α-Fe and γ-Fe phases increases where as that of $(Fe,Ni)_2B$ and $(Fe,Ni)_{23}B_6$ phases decreases. Moreover, the microstructural investigation of these alloys reveals transition of the morphology of the bimodal eutectic structure to irregular eutectic structure. These microstructural transition leads to deterioration of the plasticity of the alloys even though they contain large amount of solid solution α-Fe and γ-Fe phases. Moreover, the mechanical properties of the bimodal eutectic composites can be controlled by a change of the eutectic structure. It is suggested that the morphology of the eutectic colony in the bimodal eutectic composite plays an important role to enhance the both strength and plasticity.

Acknowledgement

This work was supported by the Global Research Laboratory (GRL) Program of Korea Ministry of Education, Science and Technology and POSCO.

References

[1] A. Inoue, Acta Mater. 48 (2000) 279.
[2] W.L. Johnson, MRS Bull. 24 (1999) 42.
[3] R.Z. Valiev, Mater. Sci. Eng. A 234 (1997) 59.
[4] H. Gleiter, Acta Mater. 48 (2000) 1.
[5] C.C. Koch, Scripta Mater. 49 (2003) 657.
[6] A.L. Greer, Science 267 (1995) 1947.
[7] C.C. Hays, C.P. Kim, W.L. Johnson, Phys. Rev. Lett. 84 (2000) 2901.
[8] C. Fan, R.T. Ott, T.C. Hufnagel, Appl. Phys. Lett. 81 (2002) 1020.
[9] Y.C. Kim, J.H. Na, J.M. Park, D.H. Kim, J.K. Lee, W.T. Kim, Appl. Phys. Lett. 83 (2003) 3093.
[10] D.G. Pan, H.F. Zhang, A.M. Wang, Z.Q. Hu, Appl. Phys. Lett. 89 (2006) 261904.
[11] G. He, J. Ekert, W. Löser, L. Schultz, Nat. Mater. 2 (2003) 33.
[12] K.B. Kim, J. Das, F. Baier, J. Eckert, J. Alloys Compd. 434 (2007) 106.
[13] J. Das, W. Löser, U. Kühn, J. Eckert, S.K. Roy, L. Schultz, Appl. Phys. Lett. 82 (2003) 26.
[14] G.A. Song, J.S. Lee, J.S. Park, N.S. Lee, W.H. Lee, K.B. Kim, J. Alloys Compd. 481 (2009) 135.
[15] L.L. Shi, H. Ma, T. Liu, J. Xu, E. Ma, J. Mater. Res. 21 (2006) 613.
[16] J.M. Park, S.W. Sohn, D.H. Kim, K.B. Kim, W.T. Kim, J. Eckert, Appl. Phys. Lett. 92 (2008) 091910.
[17] J.M. Park, S.W. Sohn, T.E. Kim, D.H. Kim, K.B. Kim, W.T. Kim, Scripta Mater. 57 (2007) 1153.
[18] J.H. Han, K.B. Kim, S. Yi, J.M. Park, S.W. Sohn, T.E. Kim, D.H. Kim, J. Das, J. Eckert, Appl. Phys. Lett. 93 (2008) 141901.
[19] J.H. Han, K.B. Kim, S. Yi, J.M. Park, D.H. Kim, S. Pauly, J. Eckert, Appl. Phys. Lett. 93 (2008) 201906.
[20] G.A. Song, W.H. Lee, N.S. Lee, J.M. Park, D.H. Kim, D.H. Kim, J.S. Lee, J.S. Park, K.B. Kim, J. Mater. Res. 24 (2009) 2891.
[21] J. Das, K.B. Kim, F. Baier, W. Lőser, J. Eckert, Appl. Phys. Lett. 87 (2005) 161907.
[22] J.M. Park, D.H. Kim, K.B. Kim, W.T. Kim, Appl. Phys. Lett. 91 (2007) 131907.